Transition metal-nitrogen co-doped carbide-derived carbon catalysts for oxygen reduction reaction in alkaline direct methanol fuel cell

Sander Ratso [a], Ivar Kruusenberg [a], Maike Käärik [a], Mati Kook [b], Rando Saar [b], Petri Kanninen [c], Tanja Kallio [c], Jaan Leis [a], Kaido Tammeveski [a,*]

[a] Institute of Chemistry, University of Tartu, Ravila 14a, 50411 Tartu, Estonia
[b] Institute of Physics, University of Tartu, W. Ostwald Str. 1, 50411 Tartu, Estonia
[c] School of Chemical Engineering, Aalto University, FI-00076, Aalto, Espoo, Finland

ARTICLE INFO

ABSTRACT

In this work, we demonstrate the electrocatalytic properties of cobalt- and iron-containing nitrogen-doped carbide-derived carbon materials in the oxygen reduction reaction (ORR) and utilise these as cathode catalysts in an alkaline direct methanol fuel cell. The carbide-derived carbon material is produced by chlorination of titanium carbide, which is then pyrolysed in the presence of dicyandiamide and either a cobalt or iron salt. The electrocatalytic activity towards the ORR and stability of the catalyst materials is tested in 0.1 M KOH solution employing the rotating disk electrode (RDE) method and compared to a commercial Pt/C catalyst. The elemental composition in the bulk of the materials is studied using energy dispersive X-ray spectroscopy and on the surface by X-ray photoelectron spectroscopy. Scanning electron microscopy is used to investigate the surface morphology of the resulting catalysts. The performance of the catalysts is also compared in alkaline direct methanol fuel cell. The catalysts' performance is comparable to that of Pt/C in both RDE and fuel cell measurements and rather peculiar morphologies are observed by the growth of carbon nanotubes during pyrolysis. Overall, these novel catalysts show great potential for application in alkaline direct methanol fuel cells.

© 2017 Elsevier B.V. All rights reserved.

1. Introduction

The energy demands of the modern society have put a great strain on the fossil fuel economy resulting in concerns over the environmental sustainability of the current energy supply systems. Many new technologies have been developed concerning storage and production of energy from cleaner and renewable resources. In several of these technologies, for example fuel cells and metal-air batteries the oxygen reduction reaction (ORR) plays a great role [1–3]. The benefits of using efficient power sources such as fuel cells, however, are currently offset by the cost and scarcity of platinum, which is used as a catalyst for ORR [4]. Platinum and Pt alloy-based catalysts are also known to be unstable over time and have other disadvantages, such as poor tolerance to carbon monoxide and methanol [5]. During the past decade there has been a massive effort towards replacing Pt-based catalysts with two main strategies emerging: using metal-free heteroatom (mainly nitrogen) doped carbon catalysts [6–8] or incorporating transition metals, most notably iron and cobalt, into the carbon structure along with heteroatoms [9–15]. Carbon nanomaterials, which are traditionally also used as a support for Pt-based ORR catalysts, have many advantages over other supports such as abundant precursors, large surface area, high electrical conductivity, chemical and mechanical stability and simple surface modification [16]. Control of the porosity, specific surface area and degree of graphitisation of the carbon material is of utmost importance in selecting suitable catalysts as these govern the mass-transfer of reactants and products and stability of catalysts in fuel cell conditions [9,17]. Carbon nanotubes [18–20], graphene [21–23], ordered mesoporous carbon [24], carbon aerogels [25–27], etc. have been used as novel carbon substrates for preparing transition metal-nitrogen-carbon (M-N-C) type catalysts for ORR.

Carbide-derived carbon (CDC), a carbon material produced by removal of non-carbon atoms from the lattice of a carbide is an excellent candidate for fuel cell applications. CDCs have easily tunable porosity and degree of graphitisation by selection of starting carbides and synthesis temperatures. Their specific surface area can be as high as $2000 \, \mathrm{m^2 \, g^{-1}}$ [28,29]. These materials are also already mass-produced with excellent and reproducible results

[30,31]. However, the application of CDCs for ORR electrocatalysis has so far mainly focused on using them as a support material for platinum [32,33]. The electroreduction of O_2 has also been investigated on undoped CDCs [34,35]. To enhance the ORR catalytic abilities of carbon nanomaterials to a level needed for use in fuel cells via the strategies previously described, a number of methods have been developed. Nitrogen-doping of carbon materials is one of the most frequently employed strategies to enhance their ORR performance. Depending on the exact position of the nitrogen atoms in carbon skeleton, four main types of nitrogen have been identified in N-doped carbon materials using X-ray photoelectron spectroscopy: pyridinic-N, which is located at the edge sites of six-member carbon rings and donates one *p*-electron to the aromatic π-systems, graphitic-N, which is linked to three carbon atoms in the carbon plane and can donate two *p*-electrons, pyrrolic-N, which occurs in a five-member carbon ring and pyridinic-N-oxide [36]. Due to the difficulties in synthesising a catalyst containing a single type of nitrogen moiety, there has been much discussion over the role of each of these types in increasing the electrocatalytic activity of carbon-based catalysts towards the ORR, with pyridinic and graphitic nitrogen considered to have the biggest positive effect [37–41]. Numerous ways to introduce these moieties into carbon materials have been developed, such as direct growth of nitrogen-containing carbon materials using chemical vapour deposition (CVD) [42], solvothermal methods [43] and nitrogen doping via pyrolysis of a precursor carbon structure [44–46] or pyrolysing a nitrogen containing compound which results in a nitrogen doped carbon structure [47,48] yielding different relative contents of the aforementioned nitrogen groups. The incorporation of transition metals (such as Co or Fe) into nitrogen-doped carbon materials further increases their electrocatalytic activity for ORR. The exact nature of catalytically active ORR sites in these catalysts is a matter of debate, with some working groups claiming that metals only increase the effectiveness of nitrogen doping and do not themselves participate in the electrocatalysis of O_2 reduction [49,50], others arguing for the existence of M-N_x active sites in these catalysts [51–53] and a third group of scientists insisting graphitic N-doped carbon on metal particles to be the most active in certain conditions [54]. In most cases, the authors have conceded that as in carbon catalysts doped with only nitrogen, the real resulting materials probably contain more than one type of active site. A variety of methods has been developed for synthesising M-N-C catalysts, with pyrolysis of a carbon support in the presence of metal salts and nitrogen-containing compounds being the most popular, although in many cases the carbon support is also formed during the synthesis step [9–11,55].

In this work, we present a procedure for synthesising a highly active catalyst containing pre-existing carbide-derived carbon and carbon nanotubes formed during the synthesis, both of which incorporate nitrogen and either Co or Fe into their structures, thus notably increasing the ORR activity of the catalyst in alkaline media. These materials are also tested as cathode catalysts of alkaline direct methanol fuel cell and compared to commercial Pt/C.

2. Experimental

2.1. Preparation of catalysts

The support carbide-derived carbon (CDC) was purchased from Skeleton Technologies (Estonia). Titanium carbide powder (TiC$_{0.5}$, H.C. Starck, 15.4 g) was loaded into a horizontal quartz-tube reactor. The reactor was purged with argon (AGA, 4.0), heated up to 800 °C and then let to react with Cl_2 gas at 800 °C for 60 min using chlorine flow of 1 l min^{-1}. After that, the CDC powder formed was annealed in Ar flow at 1000 °C for 20 h and dechlorinated deeply

in hydrogen (AGA, 4.0) flow at 800 °C for 70 min [31]. For decreasing the size of CDC grains obtained, those were ball-milled with 5 mm ZrO_2 balls [56]. Ethanol was added to the CDC material to achieve a motor-oil like viscosity along with polyvinylpyrrolidone in an amount according to 1/10 of the carbon material to enhance the milling process. The total milling time was 1 h with a speed of 800 rpm in a planetary ball-mill. The CDC material was dried, weighed and dicyandiamide in the amount of 20 times the weight of the carbon material was added in an isopropanol solution along with either $CoCl_2$ with a mass ratio of 1:20 or $FeCl_3$ with a mass ratio of 1:40 to carbon. The dispersion was then homogenised in a sonicating bath for 2 h and dried in vacuum at 75 °C. The resulting mixture was then pyrolysed in a quartz tubular oven in flowing N_2 at 800 °C for 2 h. This results in nitrogen doping from the dicyandiamide and inclusion of metal-containing active sites from the cobalt and iron. After 2 h the catalyst was quickly removed from the heating zone. To remove inactive metal phases from the catalyst it was leached in a mixture of 0.5 M H_2SO_4 and 0.5 M HNO_3 at 50 °C for 8 h. The pyrolysis step was then repeated to assure deprotonation of M-N_x centres and removal of adsorbed bisulphate from these groups. This procedure for introducing nitrogen and metals into carbon catalysts has been optimised in previous works [57–59]. In what follows, the transition metal-nitrogen co-doped CDC materials are designated as M-N-CDC (Fe-N-CDC and Co-N-CDC for iron- and cobalt-containing materials, respectively).

2.2. Surface and porosity characterisation

Scanning electron microscopy (SEM) images were taken using Helios TM NanoLab 600 (FEI) to study the surface morphology of the catalysts. Glassy carbon (GC) disks were coated with an ethanol dispersion of the catalyst materials and studied at selected magnifications to observe the surface characteristics and microstructure. To determine the bulk concentration and concentration profile of the catalysts, energy-dispersive X-ray (EDX) analysis was used with Helios NanoLab 600 electron-ion dual beam microscope equipped with a 50 mm^2 X-Max SDD detector (Oxford Instruments). The primary electron energy was 10 keV. INCA software provided by Oxford Instruments was utilised to analyse the EDX spectra.

Surface composition of the catalysts was determined via X-ray photoelectron spectroscopy (XPS). The M-N-CDC materials were dispersed in ethanol at a concentration of 2 mg ml^{-1} and pipetted onto polished GC plates or silicon wafers (1.1 × 1.1 cm). For removing the solvent the samples were heated in an oven at 60 °C. The XPS analysis was carried out using the SCIENTA SES-100 spectrometer. A non-monochromatic twin anode X-ray tube (XR3E2) with characteristic energies of 1253.6 eV (Mg K$\alpha_{1,2}$, FWHM 0.68 eV) and 1486.6 eV (Al K$\alpha_{1,2}$, FWHM 0.83 eV) was used to analyse the M-N-CDC samples. The wide scan spectra were acquired using following parameters: energy range = 800 to 0 eV, pass energy = 200 eV, step size = 0.5 eV. Following parameters for recording the high-resolution XPS spectra in the N1 s region were used: energy range = 408–392 eV, pass energy = 200 eV and step size = 0.1 eV. The analysis chamber pressure was below 10^{-9} Torr and the source power was 300 W.

The N_2 adsorption-desorption isotherms of the M-N-CDC catalyst samples were acquired at the boiling temperature of nitrogen using a NovaTouch LX2 Analyser (Quantachrome). The samples were degassed under vacuum for 12 h at 120 °C and backfilled with N_2 gas before the measurement.

2.3. Electrode preparation and electrochemical characterisation

The rotating disk electrode (RDE) method was used to investigate the electrocatalytic activity of the M-N-CDC catalyst towards the ORR. The RDE polarisation curves were measured using six

different electrode rotation rates (ω): 4600, 3100, 1900, 960, 610 and 360 rpm. The rotation speed of electrodes was controlled using a CTV101 speed control unit connected to an EDI101 rotator (Radiometer). The experiments were carried out in a 0.1 M KOH-filled (p.a. quality, Merck) three-electrode electrochemical cell at room temperature (23 ± 1 °C). Prior to the experiments the solution was saturated with O_2 (99.999%, AGA) or Ar (99.999%, AGA) and a gas flow was maintained over the solution during the experiments. A platinum spring separated from the cell by a glass frit was used as the counter electrode and a saturated calomel electrode (SCE) served as the reference electrode. All the potentials are referred to this electrode. An Autolab potentiostat/galvanostat PGSTAT30 (Metrohm Autolab, The Netherlands) was used to control the experiments via General Purpose Electrochemical System (GPES) software. A potential scan rate (ν) of 10 mV s^{-1} was used for RDE testing.

GC disks (GC-20SS, Tokai Carbon) polished to a mirror finish with 1 and 0.3 μm alumina slurries (Buehler) with a geometric area (A) of 0.2 cm^2 were pressed into a Teflon holder to serve as electrode substrates. The GC electrodes were sonicated in both 2-propanol and Milli-Q water for 5 min to remove polishing debris. The M-N-CDC materials were dispersed in ethanol (1 mg ml^{-1}) containing 0.125% FAA3 ionomer (Fumatech, 12 wt.% FAA3 in N-methyl-2-pyrrolidone) and pipetted onto the GC disk electrodes. Prior to modification of the electrodes the suspensions were homogenised via sonication for 1 h 20 μl of the catalyst suspension was transferred on the GC surface in 5 μl fractions to cover the surface uniformly and was allowed to dry in air. The catalyst loading for all the materials was thus 0.1 mg cm^{-2}.

A Pt/C catalyst was studied in similar conditions to compare it to M-N-CDC materials. The commercial 60 wt.% Pt catalyst supported on high surface area carbon was purchased from Alfa Aesar and dispersed in ethanol (1 mg catalyst ml^{-1}) in the presence of FAA3 ionomer. The Pt loading on the GC electrode was thus 20 μg cm^{-2}.

The stability tests were also carried out in O_2-saturated 0.1 M KOH. A 1000 potential cycles were measured at a potential scan rate of 100 mV s^{-1} and RDE polarisation curves were recorded after each 100 cycles at 1900 rpm and 10 mV s^{-1}. For assessing the methanol tolerance of the catalysts in the RDE mode, these were first tested in O_2-saturated 0.1 M KOH at 1900 rpm and 10 mV s^{-1}. Then methanol was added to the electrolyte solution to rise the MeOH concentration to 3 M and the catalysts were tested again using the same parameters. For comparison the methanol tolerance was also tested using a commercial 60 wt.% Pt/C.

2.4. MEA preparation and alkaline DMFC measurements

Fuel cell testing was made with the Fe-N-CDC and Co-N-CDC catalysts as well as commercial Pt/C (60 wt.% Pt, Alfa Aesar) as the cathode catalysts. Commercial PtRu/C (40 wt% Pt, 20 wt% Ru, Alfa Aesar) was used as the anode catalyst. MEA preparation was done as previously reported [57]. Shortly, catalyst inks were prepared by mixing the catalyst with isopropanol and 12 wt.% solution of FAA3 ionomer (Fumatech) in N-methyl-2-pyrrolidone (NMP). The resulting slurry was painted on woven carbon cloth gas diffusion layer (GDL, FuelCellEtc GDL-CT, thickness 410 μm) with a microporous layer (30 wt% Teflon) by an air brush (Badger 100-3-GF) and dried in a vacuum oven. The catalyst loadings were 1.73 mg cm^{-2} on the Fe-N-CDC cathode, 1.83 mg cm^{-2} on the Co-N-CDC cathode and 1.27 mg$_{Pt}$ cm^{-2} on the Pt/C cathode. The PtRu loading on the anode was 4.25 ± 0.10 mg$_{PtRu}$ cm^{-2}. The ionomer content in the catalyst layers was 30 wt.% of the total electrode mass.

The alkaline DMFC testing conditions were also similar to our previous study [57]. The fuel cell electrode area was 5.29 cm^2. A FAA3 membrane (Fumatech, thickness 50 μm, ion-exchange capacity 2 meq g^{-1}) was ion-exchanged in 0.5 M NaOH with stirring for

1 h and washed in deionised water several times. The cell was assembled with the membrane and the carbon cloth electrodes placed inside and tightened to 5 Nm. The cell temperature was 50 °C and dry O_2 (AGA, 99.999%) was fed to the cathode at a flow rate of 200 ml min^{-1} during all fuel cell measurements. The fuel solution at the anode was first 1 M methanol at 0.2 ml min^{-1}. The cell was let to stabilise until the open circuit voltage (OCV) did not change and then polarisation curves from OCV to 0.05 V ($\nu = 3$ mV s^{-1}) were measured until reproducible performance was achieved. Then the fuel solution was changed to 1 M methanol in 0.1 M KOH and the measurement procedure repeated. The cell voltage and current were controlled by a Metrohm Autolab PGSTAT302N potentiostat with a BOOSTER20A booster.

3. Results and discussion

3.1. Physical characterisation of M-N-CDC materials

The surface characteristics and morphology were studied with scanning electron microscopy (Fig. 1a,b). A characteristic area of the Fe-N-CDC sample is shown in Fig. 1a, with many CDC particles with a wide variety of sizes visible. In addition to the doped CDC material, there are numerous carbon nanotubes, which are formed from DCDA with the iron nanoparticles acting as a catalyst for nanotube growth. The wrinkled carbon layers probably also contain numerous Fe nanoparticles covered with graphitic layers which are stable and not removed by acid leaching. The carbon nanotubes improve the stability of the otherwise highly amorphous CDC material and also change the mass-transfer properties in the catalyst layer.

The channels between larger M-N-CDC grains improve the mass transport in the catalyst layer, which is very important in fuel cell applications and the microporous structure ensures efficient ORR electrocatalysis. Fig. 1b shows the surface morphology of the Co-N-CDC catalyst, with the crumpled morphology more clearly visible.

N_2 physisorption was used to study the specific surface area and porosity of the transition metal-containing nitrogen-doped CDC catalysts. The M-N-CDC catalysts' specific surface area (S_{BET}) was calculated according to the Brunauer-Emmett-Teller (BET) theory up to a nitrogen relative pressure of $P/P_0 = 0.2$. The total volume of pores (V_{tot}) was measured near to saturation pressure of N_2 ($P/P_0 = 0.97$). The microporosity (V_μ) was calculated from t-plot method using deBoer statistical thickness. The average diameter of pores (d_p) was calculated for a slit-type pore geometry using the following equation: $d_p = 2 V_{tot}/S_{BET}$. The calculations of pore size distribution (PSD) from N_2 isotherms were done by using a quenched solid density functional theory equilibria model for slit type pore. The BET area and porosity of catalyst materials is given in Table 1. The porosity characteristics for the two catalysts are fairly similar, with the Fe-N-CDC catalyst having higher microporosity than the Co-N-CDC catalyst and a somewhat smaller total pore volume and average pore size.

N_2 adsorption-desorption isotherms, presented in Fig. 2a, have a typical shape of combined Type I and II adsorption branches, which is often found for micro-mesoporous carbons [60]. For comparative purposes, we have also included the isotherms of our previously studied N-CDC material [56]. All three isotherms contain the hysteresis loop of Type H4 with the sharp step-down of the desorption branch at $P/P_0 \sim 0.4$–0.45. Comparison to N-CDC isotherm confirms that the doping with metal has no effect on the mesoporous part of the parent carbon, however, it reduces the volume of micropores. Interestingly, the total pore volume is almost equal for the N-CDC and M-N-CDC catalysts. With highly porous catalysts it is interesting to compare the pore size distributions, which are shown in Fig. 2b. The PSD for the M-N-CDC catalysts is nearly the same, with Fe-N-CDC having somewhat more pores with a width under 1 nm
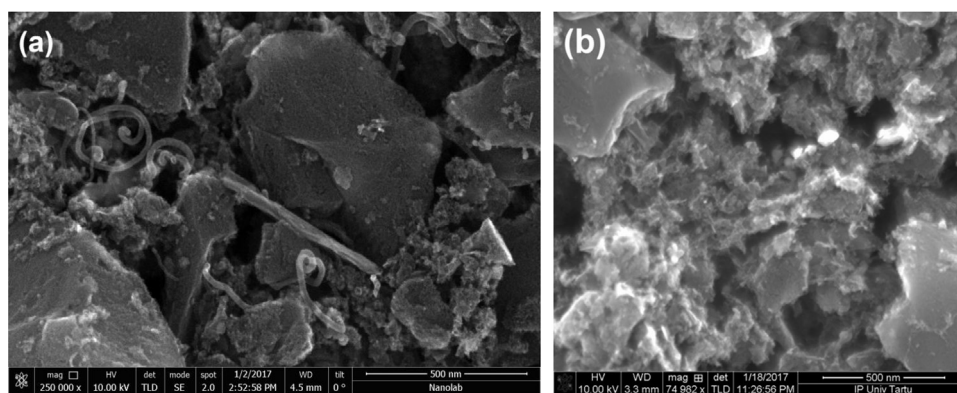
Fig. 1. SEM images of (a) Fe-N-CDC and (b) Co-N-CDC catalysts.

Table 1

Textural properties of M-N-CDC materials: BET surface area (S_{BET}), pore volume (V_{tot}), micropore volume (V_μ) and average pore size (d_p).

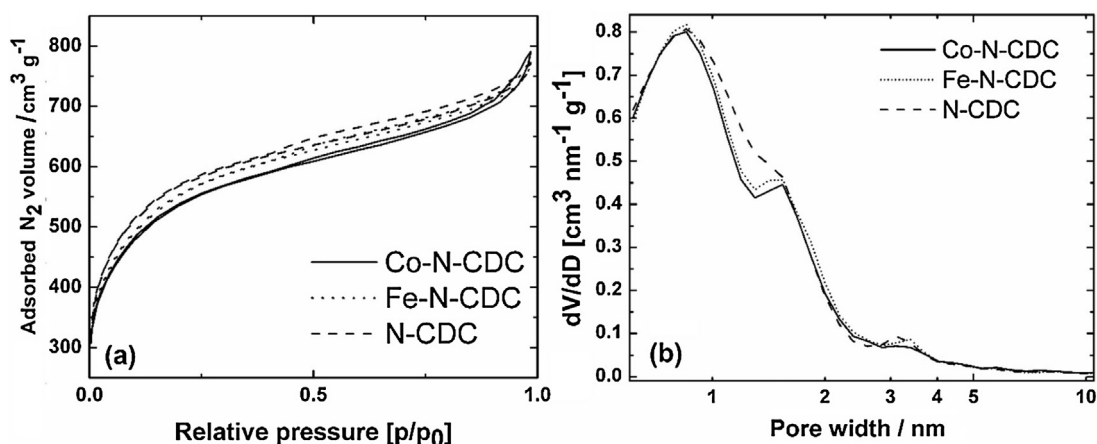| Catalyst	S_{BET}, m^2 g^{-1}	V_μ, cm^3 g^{-1}	V_{tot}, cm^3 g^{-1}	d_p, nm
Co-N-CDC	1908	0.834	1.165	1.22
Fe-N-CDC	1966	0.908	1.153	1.17

Fig. 2. Comparison of N$_2$ adsorption-desorption isotherms (a) and pore size distributions (b) for Co-N-CDC, Fe-N-CDC and N-CDC samples.

and also in the 3–4 nm range. When compared to N-CDC, however, it is apparent that many of the pores sized between 1 and 1.5 nm have been filled in the case of M-N-CDC catalysts. The reason is likely M-N$_x$ centres filling the pores in this size range, which could be useful for further choice of CDCs, a maximum number of pores of this size should give a larger number of M-N$_x$ sites in the resulting catalyst using DCDA and metal salt as the doping materials. This finding is in accordance with previous studies [61], which found the optimum pore size for active sites to be between 0.5 and 2 nm, but further narrows down the range.

The overall nitrogen content in Fe-N-CDC was 4.08 at.% and the iron content was 1.39 at.% on the basis of the EDX analysis, which indicates that a significant amount of the iron is dissolved during the acid leaching procedure. The remaining iron is in the form of either M-N$_x$ centres or iron nanoparticles covered by graphitic layers making it resistant to removal by acid washing. In the Co-N-CDC material, the nitrogen content was 5.30 at.% and the cobalt content was only 0.65 at.% in the resulting catalyst, however, noting a lower stability of the cobalt phases towards acid leaching. This is likely because of the smaller amount of carbon nanotubes formed during the pyrolysis step. Metal nanoparticles inside carbon nanotubes are known to be very stable towards acid treatment.

To assess the elemental composition near the surface of the M-N-CDC catalysts, polished Si plates were covered with the catalyst materials and the XPS measurements were undertaken. Fig. 3a–c show the results of Co-N-CDC XPS testing and Fig. 3d–f the results of the XPS analysis of Fe-N-CDC catalyst. Fig. 3a presents the XPS survey spectra for Co-N-CDC, which revealed four recognisable peaks according to the binding energy (BE) values for C1s, N1s, O1s and Co2p. The overall content of oxygen in the surface layer of the catalyst was 1.81 at.%, while the nitrogen content was 4.19 at.% and the cobalt content 0.42 at.%. The N1s high-resolution XPS spectrum for Co-N-CDC is presented in Fig. 3b and has been deconvoluted into four components to determine the relative content of different types of nitrogen: pyridinic-N-oxide (BE = 404.2 eV), graphitic-N (BE = 401.2 eV), pyrrolic-N (BE = 399.9 eV) and pyridinic-N (BE = 398.2 eV) [36]. The relative content of graphitic-N, which corresponds to N atom linked to three carbons in a six-member cycle and is considered one of the nitrogen moieties most active towards the ORR was 23.2% in this catalyst. The relative content of the other active type, pyridinic-N, was 50.2%, but this also includes the contribution from Co-N$_x$ sites [62]. The relative contents of two of the other types, pyrrolic-N and pyridinic-N-oxide, were 16.6% and 10.1%, respectively.
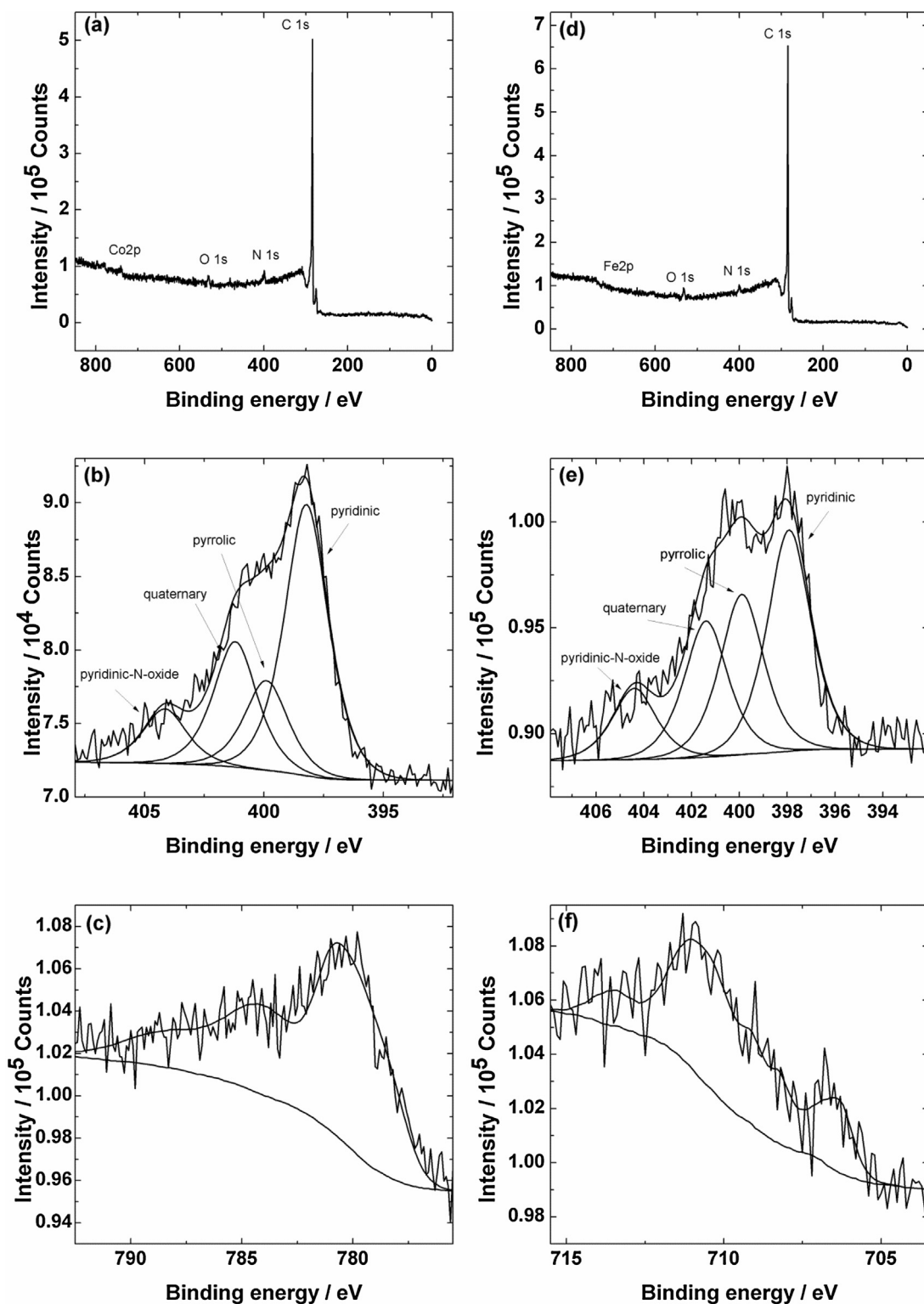
Fig. 3. XPS wide scan spectra (a,d) and core-level spectra in the N1 s (b,e), Co2p (c) and Fe2p (f) regions, for Co-N-CDC and Fe-N-CDC samples, respectively.

Table 2
Relative content of different nitrogen species in Co-N-CDC and Fe-N-CDC samples (%).

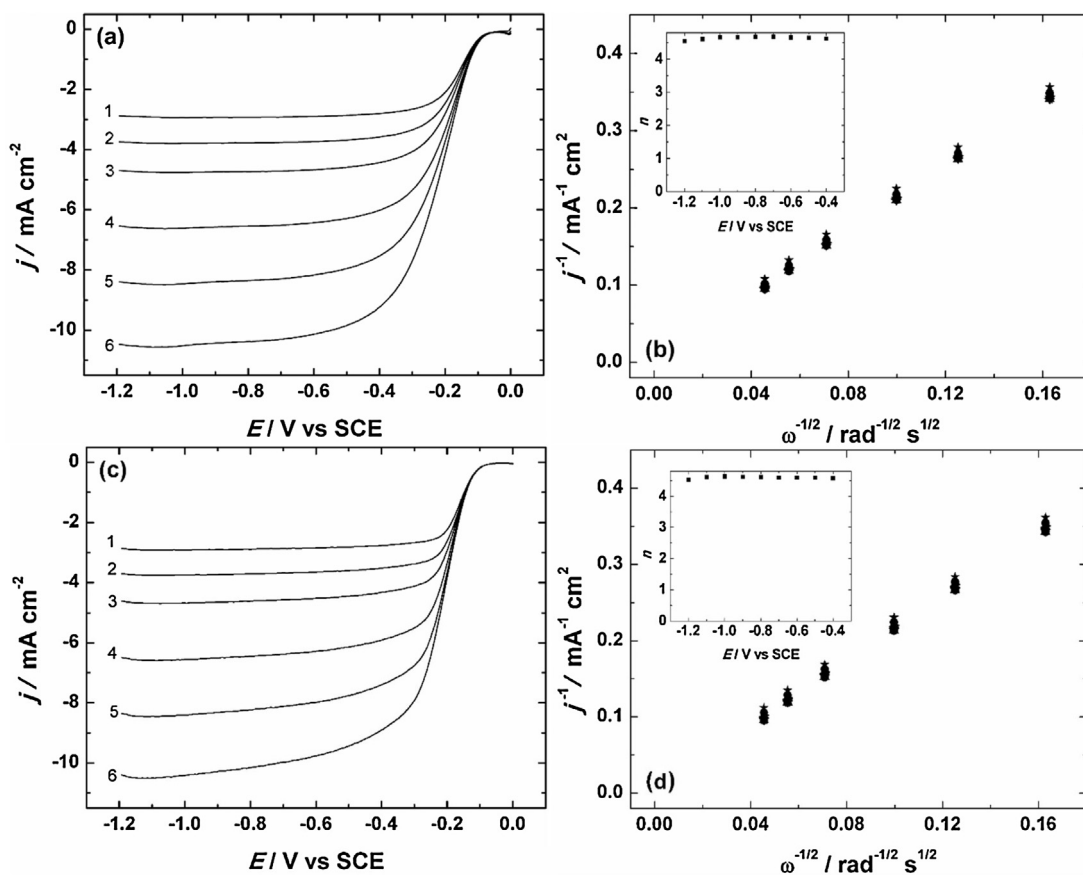| Catalyst	Pyridinic-N	Pyrrolic-N	Quaternary-N	Pyridine-N-oxide
Co-N-CDC	50.2	16.6	23.2	10.1
Fe-N-CDC	37.6	27.2	23.1	12.1

Fig. 4. RDE polarisation curves for oxygen reduction reaction on (a) Fe-N-CDC and (c) Co-N-CDC modified GC electrodes in O_2-saturated 0.1 M KOH. $\nu = 10\,mV\,s^{-1}$, $\omega =$ (1) 360, (2) 610, (3) 960, (4) 1900, (5) 3100 and (6) 4600 rpm. K-L plots for O_2 reduction on (b) Fe-N-CDC and (d) Co-N-CDC catalysts in 0.1 M KOH. Inset shows the potential dependence of n.

The XPS survey spectrum for Fe-N-CDC material, which also consisted of four distinct peaks, is presented in Fig. 3d. In this case the Fe2p peak is not very well visible as the iron content in the surface layer was only 0.14 at.%. The oxygen content was 2.23 at.% and the nitrogen content 2.51 at.% in this sample. The deconvoluted N1 s XPS peak for Fe-N-CDC is shown in Fig. 3e. The relative content of pyridinic-N in this catalyst was determined to be 37.6% and the graphitic-N content 23.1%, while the relative contents of pyridinic-N-oxide and pyrrolic-N were 12.1% and 27.2%, respectively. For a better overview, the relative contents of different nitrogen moieties in the M-N-CDC catalysts are listed in Table 2.

The high-resolution Co2p and Fe2p XPS spectra are presented in Figs. 2c and f, but due to the serious difficulties in the deconvolution of these spectra and the low signal-to-noise ratio it was not possible to determine the exact configurations for Co and Fe. It is interesting to note that the catalyst material containing cobalt had a much larger relative content of pyridinic nitrogen than its iron-containing counterpart and both metals changed the relative contents for different types of nitrogen when compared to a similar CDC material doped with only nitrogen [56]. However, both metals induced the nitrogen content to be much higher in the surface layer of the material, which may increase the overall ORR activity of the catalysts.

3.2. Electrochemical characterisation of M-N-CDC catalysts

The rotating disk electrode method was employed to investigate the electrocatalytic activity of transition metal-containing nitrogen-doped CDC catalysts towards the oxygen reduction reaction in 0.1 M KOH solution. The ORR electrocatalytic activity of the

CDC material used as a precursor has been studied in our previous work [56]. Fig. 4a shows the O_2 reduction polarisation curves for a GC electrode modified with Fe-N-CDC catalyst. The onset potential of the ORR (E_{onset}) for this catalyst is ca. −0.1 V vs SCE, which is 50 mV more positive as compared our previously studied N-doped CDC material. This shows the effect of adding transition metal to the catalyst: the Fe-N_x sites and iron particles covered with nitrogen-doped graphitic layers facilitate oxygen reduction and shift the O_2 reduction wave somewhat more positive as compared to metal-free N-doped CDC materials. The reduction current values are also rather high for such a low catalyst loading. Fig. 4b demonstrates the Koutecky-Levich (K-L) plots derived from the ORR polarisation curves with the electron transfer number (n) shown in the inset. The n values were calculated from the K-L equation [63]:

$$\frac{1}{j} = \frac{1}{j_k} + \frac{1}{j_d} = -\frac{1}{nFkc_{O_2}^b} - \frac{1}{0.62nFD_{O_2}^{2/3}\nu^{-1/6}\omega^{1/2}c_{O_2}^b} \tag{1}$$

where j is the experimentally measured current density, j_k and j_d are the kinetic and diffusion limited current densities, respectively, k is the electrochemical rate constant for the reduction of O_2 (cm s^{-1}), F is the Faraday constant (96,485 C mol^{-1}), ω is the electrode rotation rate (rad s^{-1}), D_{O_2} is the diffusion coefficient of O_2 in 0.1 M KOH (1.9×10^{-5} cm^2 s^{-1}) [64], C_{O_2} is the solubility of O_2 in 0.1 M KOH (1.2×10^{-6} mol cm^{-3}) [64] and ν is the kinematic viscosity of the solution (0.01 cm^2 s^{-1}) [65].

The K-L plots yield an intercept close to zero, indicating a diffusion-limited ORR process taking place on this catalyst. The n values are close to four or even slightly above, which is proof of a 4-electron reduction of oxygen on Fe-N-CDC catalysts. The values
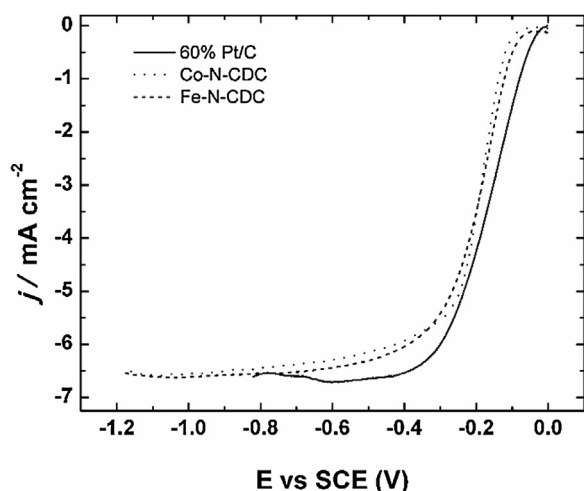
Fig. 5. A comparison of the RDE results of O_2 reduction on Fe-N-CDC, Co-N-CDC and commercial 60% Pt/C modified GC electrodes in O_2-saturated 0.1 M KOH solution. $\nu = 10$ mV s^{-1}, $\omega = 1900$ rpm.

of n over 4 can be explained by the structure of the catalyst layer on a GC electrode being somewhat uneven and the catalyst itself being highly porous. This could lead to slightly non-laminar electrolyte solution flows in the RDE mode. The electrochemical oxygen reduction behaviour of the Co-N-CDC catalyst presented in Fig. 4c, is very similarly to that of Fe-N-CDC, with the E_{onset} value being somewhat more negative on this catalyst. It is interesting that even though, as identified by the XPS analysis, these catalysts have very different nitrogen and metal content on the surface, their overall electrocatalytic ORR activity is basically the same. The surface-to-bulk ratio of cobalt content in Co-N-CDC material is much higher than surface-to-bulk ratio of iron in Fe-N-CDC, which is due to a larger amount of nitrogen doped carbon-coated iron particles and carbon nanotubes formed during the pyrolysis in Fe-N-CDC visible from the SEM images. As the iron particles covered in carbon do not give an iron signal in XPS, the bulk content determined by EDX and the surface content determined by XPS differ much more in this case than in Co-N-CDC. These phases are also more stable in acid, which causes the metal content in the final Fe-N-CDC catalyst to be higher than in Co-N-CDC even though the starting metal concentration was twice as high. Co-N-CDC also demonstrates high O_2 reduction currents and a value of n close to 4 (Fig. 4d), meaning that O_2 is reduced to water via 4-electron pathway on this catalyst. Interestingly, the relative contents of the two nitrogen surface species known to be active (graphitic and pyridinic nitrogen) are rather different in both catalysts, but result in a similar ORR electrocatalytic activity. As can be seen, the fact that the transition metal and nitrogen are much more homogeneously distributed in Fe-N-CDC plays little role in the RDE testing of electrocatalyst materials, but during DMFC testing the effect is much more prominent.

Fig. 5 displays a comparison of the ORR activity of transition metal-containing N-doped CDC catalysts and a commercial 60 wt.% Pt/C catalyst in O_2-saturated 0.1 M KOH. Both of the M-N-CDC catalysts behave very similarly, with the E_{onset} value ca. 100 mV more negative than that of the commercial carbon-supported Pt catalyst and half-wave potentials ($E_{1/2}$) ~50 mV more negative. As the difference in the ORR electrocatalytic activity is rather small, but the price of the M-N-CDC materials is much lower, these catalysts have excellent potential to rival Pt/C in alkaline fuel cells. As metal-containing nitrogen-doped porous carbon materials have been extensively studied already, it is important to compare our catalysts to previously developed materials [66]. The most popular strategies are using either a nitrogen-containing polymer, metal-organic frameworks (MOF) or silica structures as a template for

preparing catalysts with an ordered porous structure [67]. Jiang et al. demonstrated a metal-containing nitrogen-doped catalyst synthesised from Co and Fe porphyrins to be active in both acidic and alkaline conditions [68]. The overall ORR activity of their catalyst was very similar to the catalysts presented in this work, but the catalyst loading used was 10 times higher than that used in this work. Gokhale et al. also synthesised a catalyst with similar activity to M-N-CDCs using the pyrolysis of ethylenediaminetetraacetic acid ferric sodium salt [69]. The price of this catalyst is also in the same class as the materials presented here, however the loading used is 6 times higher, which might prove to be a problem when going from the RDE testing to real fuel cells experiments. The applicability of MOF-based catalysts in alkaline media was studied by Ge et al., who produced a carbon nanotube-MOF composite [70] with high electrocatalytic activity towards the ORR in O_2-saturated 0.1 M KOH. The ORR activity of this catalyst was again comparable to M-N-CDCs, but the loading was nearly 8 times higher, proving the advantage of a CDC based material as compared to MOFs. Another very active MOF-derived catalyst was developed by Strickland et al., with no direct iron-nitrogen coordination, but very high activity surpassing that of M-N-CDCs, albeit at a catalyst loading 6 times higher [54]. The Fe-N-CDC contains multiple types of ORR active sites including N-doped carbon encapsulated iron nanoparticles, which may be preferable for maximum activity towards the ORR in contrast to this catalyst. The silica-substrate process has been demonstrated to yield active ORR catalysts by Sun et al., who used pyrolysis of a polymer, DCDA and cobalt nitrate templated into colloidal silica spheres to produce their material, which was very active at a rather low loading compared to most catalysts in the literature (0.22 mg cm^{-2}), which is still more than twice higher than that used in this work [71]. The superior activity of Co-N-CDC is most likely due to a much higher specific surface area and microporosity. The increase in the ORR activity with rising BET surface area was also confirmed by Müllen's work group, who used a silica colloid as a framework during the pyrolysis step, but their catalysts were also more mesoporous and less active than M-N-CDCs at a similar loading [62].

The stability of the M-N-CDC catalysts was also tested with a modified glassy carbon RDE in oxygen-saturated 0.1 M KOH. The catalysts were tested during 1000 cycles from 0 to −1.2 V vs. SCE (Fig. 6). The E_{onset} and $E_{1/2}$ values remained the same during the whole testing period, with a rather minimal change in the limiting current values, proving the stability of both of these materials in alkaline conditions. In fuel cell the conditions can however be somewhat different, as the mass transfer process is much more dominated by the porosity of the catalyst in fuel cells. A large amount of micropores might be favourable to achieve high starting activity [72], but also contributes to a rapid loss in activity of the catalysts due to mass-transfer losses, which are especially apparent in fuel cell conditions as the catalyst layer is thick [55]. The carbon nanotubes between N-doped CDC grains in the M-N-CDC catalysts presented in this work, however, prevent this by creating channels which facilitate mass transport without a loss in activity as the in-situ formed carbon nanotubes themselves are also highly active towards the ORR [73]. This means the M-N-CDC materials have excellent potential to replace Pt as a cathode catalyst in low-temperature fuel cells, such as alkaline direct methanol fuel cells. To prove the suitability of these materials in real alkaline DMFCs, they were both tested as the cathode catalyst and compared to the performance of the commercial 60 wt% Pt/C material.

In alkaline DMFC, one of the key problems with Pt-based catalysts is the crossover of methanol through the anion exchange membrane from the anode side of the cell onto the cathode, which results in a fuel loss in the cathode area and a mixed electrode potential [74]. To eliminate this possibility in our fuel cell testing, we first studied the methanol tolerance of the Co-N-CDC and Fe-
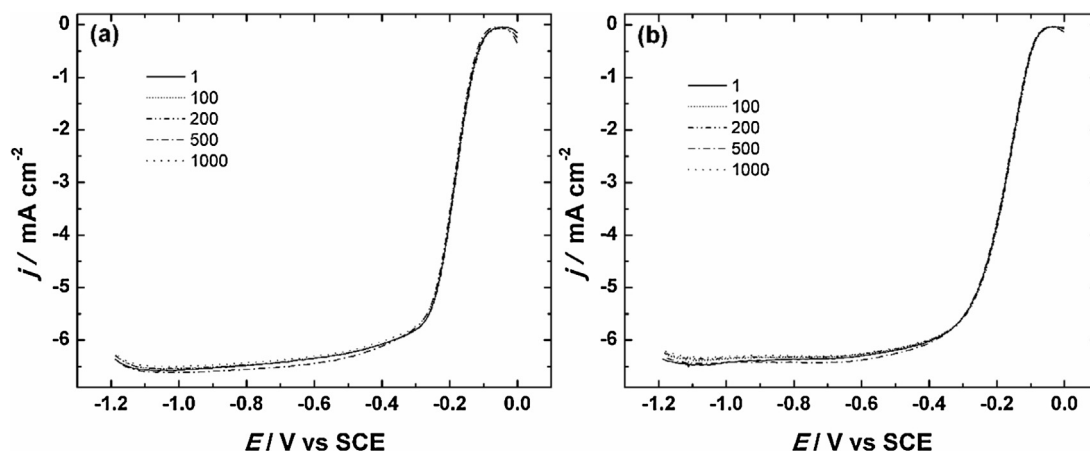
Fig. 6. The stability of (a) Co-N-CDC and (b) Fe-N-CDC modified GC electrodes in O_2-saturated 0.1 M KOH solution during 1000 potential cycles. $\nu = 10$ mV s^{-1}, $\omega = 1900$ rpm.
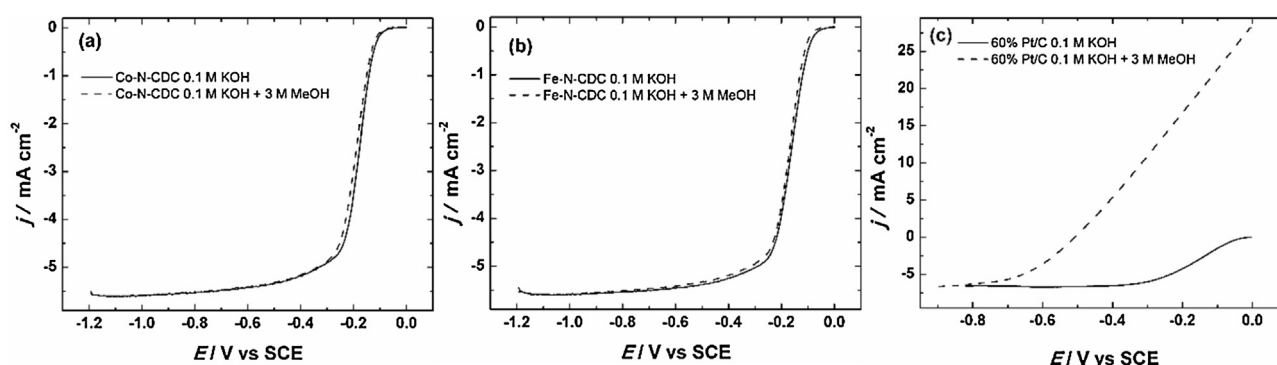

Fig. 7. ORR polarisation curves for (a) Co-N-CDC, (b) Fe-N-CDC and (c) 60 wt.% Pt/C modified GC electrodes in O_2-saturated 0.1 M KOH solution with and without 3 M MeOH. $\nu = 10$ mV s^{-1}, $\omega = 1900$ rpm.

N-CDC catalysts in 0.1 M KOH solution which also contained 3 M methanol. As can be seen from Fig. 7, the methanol addition has very little effect on the ORR activity of the M-N-CDC catalysts and as such the effect of methanol crossover should be negligible. The dramatic effect of methanol addition on the commercial Pt/C catalyst is demonstrated in Fig. 7c. It is clear that methanol crossover would be a major problem when using Pt/C in comparison to the M-N-CDC catalysts.

3.3. DMFC performance

Alkaline DMFC testing was performed with Fe-N-CDC, Co-N-CDC and commercial Pt/C catalysts. The measured polarisation and power density curves are presented in Fig. 8, normalised to both the fuel cell area (Fig. 8a–b) and cathode catalyst mass (Fig. 8c–d). The fuel was 1 M methanol solution in both deionised water and 0.1 M KOH.

Without 0.1 M KOH, the performance of the DMFC is mediocre and Pt/C performs better than Co- and Fe-N-CDC. The maximum power densities are 2.07 mW cm^{-2} or 1.63 W g$_{Pt}^{-1}$ at 0.20 V for Pt/C; 1.46 mW cm^{-2} or 0.84 W g$_{Fe-N-CDC}^{-1}$ at 0.24 V for Fe-N-CDC and 1.43 mW cm^{-2} or 0.78 W g$_{Co-N-CDC}^{-1}$ at 0.23 V for Co-N-CDC. The poor performance can be attributed to the fact that CO_2 is produced from methanol at the anode and it will convert to negatively charged HCO_3^- in water [75]. This will then neutralise the MEA by replacing OH$^-$ in the membrane and ionomer affecting also the cathode environment. Furthermore, the conductivity of the system is lowered by the replacement of OH$^-$ with HCO_3^-. Pt/C is generally a good ORR catalyst in all environments and can function better than the synthesised catalysts in these challenging neutral

conditions. However, the methanol tolerance of Fe- and Co-N-CDC can be observed from the high OCV compared to Pt/C (0.69 and 0.64 V versus 0.60 V). This allows the maximum power density to be reached at a higher potential, which is important for applications requiring a minimum voltage to work. The origin of activity in DMFC is related again to M-N$_x$ centres and metal particles covered in nitrogen-doped graphitic layers, although in a recent work Yan et al. also found that epoxy groups increase the activity of iron-containing catalysts when exposed to methanol [76]. Another property which has been shown to have a large positive effect on the activity of a catalyst in an alkaline DMFC is a high specific surface area: Sun et al. recently found a correlation between the increase of surface area and performance in a DMFC using heteroatom-doped black pearls [77], although the opposite effect was found in a different work [78]. The microporous characteristic of the M-N-CDC catalysts also plays a role in ORR in alkaline DMFCs, as shown by Zhao et al. in their work on MOF-based catalysts [79]. The performance they obtained exceeds that of the M-N-CDC in our tests, but the catalyst loading in their case is nearly twice as high.

Nevertheless, the addition of 0.1 M KOH to the fuel solution dramatically improves the DMFC performance as the membrane and the ionomer remain in OH$^-$ form during operation. The more alkaline environment is better suitable for the M-N-CDC catalysts and the performance is noticeably increased. A linear rise with alkali concentration has been reported in previous works due to the rise of ionic conductivity in the membrane and more alkaline conditions [80,81]. It is clear that Fe-N-CDC performs even better than Pt/C when 0.1 M KOH is added: the maximum power densities are 4.70 mW cm^{-2} or 3.70 W g$_{Pt}^{-1}$ at 0.17 V for Pt/C; 6.85 mW cm^{-2} or 3.96 W g$_{Fe-N-CDC}^{-1}$ at 0.30 V for Fe-N-CDC and 6.21 mW cm^{-2}

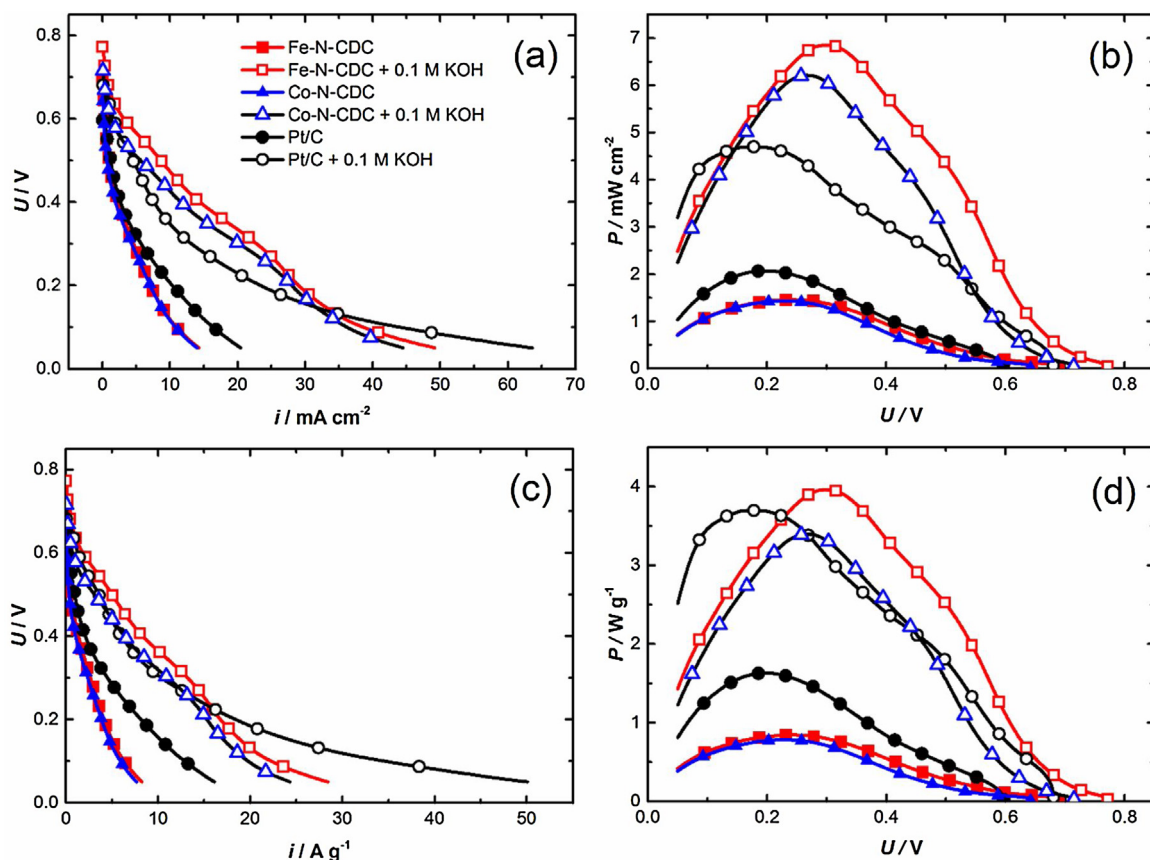**Fig. 8.** DMFC performances of Fe-N-CDC (red squares, 1.73 mg $_{Fe-N-CDC}$ cm^{-2}), Co-N-CDC (blue triangles, 1.83 mg$_{Co-N-CDC}$ cm^{-2}) and Pt/C (black circles, 1.27 mg $_{Pt}$ cm^{-2}) catalysts in alkaline DMFC with a Fumatech FAA3 membrane (50 °C). At the anode (0.2 ml min^{-1}): 1 M methanol (filled symbols) and 1 M methanol with 0.1 M KOH (empty symbols). At the cathode: pure dry O$_2$ (200 ml min^{-1}). (a) Current density and (b) power density normalised to fuel cell area. (c) Current density and (d) power density normalised to the mass of Pt and Fe-N-CDC or Co-N-CDC at the cathode. (For interpretation of the references to colour in this figure legend, the reader is referred to the web version of this article.)

or 3.40 W g$_{Co-N-CDC}$$^{-1}$ at 0.27 V for Co-N-CDC. In the case of Fe-N-CDC, this indicates a remarkable 7% increase compared to Pt/C in mass specific performance with a catalyst made from cheap and abundant raw materials. It also outperformed many of the catalysts tested in similar conditions, but where no KOH was added, including our previous works [76,82–84]. The current and power densities for Fe-N-CDC are especially high in the whole voltage region from OCV to 0.2 V indicating a low activation overpotential and the benefit from methanol tolerance. This can also be seen from the OCVs, which are almost 0.1 V higher than without KOH (0.68 and 0.77 V for Pt/C and Fe-N-CDC, respectively). At very high current density region, Pt/C performs better possibly due to mass transfer losses in the non-optimised catalyst layer with Fe-N-CDC. Co-N-CDC behaves similarly but the overall performance is lower than with Fe-N-CDC as is expected from the RDE measurements. The absolute performances are not as impressive as in some alkaline DMFC studies [75,79,85,86] and especially acidic DMFC results [87–89], however, this is due to the low KOH concentration (0.1 M) we used to have better correspondence to RDE conditions, relatively low catalyst loading (1.73 mg cm^{-2}) and the restricted operating temperature (50 °C) due to FAA3 membrane. It must also be noted that in all of these works the catalyst layer preparation and ionomer content has been optimised further, as witnessed by the higher current densities achieved with commercial catalysts. Yet, in this system the Fe-N-CDC performs better than commercial Pt/C and thus shows excellent potential as a cheap and highly effective ORR catalyst in fuel cells. A thorough analysis of the results attained recently for DMFCs is available in the literature [90].

These results highlight the great potential of non-precious metal catalysts for electrochemical energy conversion. The demand for efficient, stable, tolerant and cheap catalyst materials for replacing the expensive and diminishing Pt for ORR is only going to increase as fuel cells gain popularity. We have now shown that even higher mass specific performance than Pt can be achieved with our stable and tolerant Fe-N-CDC catalyst using only abundant and cheap raw materials promising sustainable and affordably energy for the requirements of the future.

4. Conclusions

Transition metal-containing nitrogen-doped carbide derived carbon materials were synthesised using the pyrolysis of metal salts and dicyandiamide in the presence of CDCs. The oxygen electroreduction activity of these catalysts rivalled that of 60% Pt/C in alkaline conditions and physical characterisation methods revealed growth of interlinking carbon nanotubes between the CDC particles during pyrolysis, which created a beneficial microporous structure with mesoporous channels containing carbon nanotubes in between. This structure facilitated the oxygen reduction reaction in the catalysts and allowed them to achieve activities near to the commercial Pt/C catalyst along with stability over 1000 potential cycles. The transition metal-containing nitrogen-doped CDCs were tested as cathode catalysts of alkaline DMFC and Fe-N-CDC showed the best performance, surpassing that of 60% Pt/C.

Acknowledgements

References

[1] M.Z. Jacobson, W.G. Colella, D.M. Golden, Science 308 (2005) 1901–1905, http://dx.doi.org/10.1126/science.1109157.

[2] V. Neburchilov, H. Wang, J.J. Martin, W. Qu, J. Power Sources 195 (2010) 1271–1291, http://dx.doi.org/10.1016/j.jpowsour.2009.08.100.

[3] I. Katsounaros, S. Cherevko, A.R. Zeradjanin, K.J.J. Mayrhofer, Angew. Chem. Int. Ed. 53 (2014) 102–121, http://dx.doi.org/10.1002/anie.201306588.

[4] M.K. Debe, Nature 486 (2012) 43–51, http://dx.doi.org/10.1038/nature11115.

[5] R.W. Reeve, P.A. Christensen, A.J. Dickinson, A. Hamnett, K. Scott, Electrochim. Acta 45 (2000) 4237–4250, http://dx.doi.org/10.1016/S0013-4686(00)00556-9.

[6] N. Daems, X. Sheng, I.F.J. Vankelecom, P.P. Pescarmona, J. Mater. Chem. A 2 (2014) 4085–4110, http://dx.doi.org/10.1039/c3ta14043a.

[7] L. Dai, Y. Xue, L. Qu, H.J. Choi, J.B. Baek, Chem. Rev. 115 (2015) 4823–4892, http://dx.doi.org/10.1021/cr5003563.

[8] K.N. Wood, R. O'Hayre, S. Pylypenko, Energy Environ. Sci. 7 (2014) 1212–1249, http://dx.doi.org/10.1039/c3ee44078 h.

[9] G. Wu, A. Santandreu, W. Kellogg, S. Gupta, O. Ogoke, H. Zhang, H.L. Wang, L. Dai, Nano Energy 29 (2016) 83–110, http://dx.doi.org/10.1016/j.nanoen.2015.12.032.

[10] F. Jaouen, E. Proietti, M. Lefèvre, R. Chenitz, J.-P. Dodelet, G. Wu, H.T. Chung, C.M. Johnston, P. Zelenay, Energy Environ. Sci. 4 (2011) 114, http://dx.doi.org/10.1039/c0ee00011f.

[11] Z. Chen, D. Higgins, A. Yu, L. Zhang, J. Zhang, Energy Environ. Sci. 4 (2011) 3167–3192, http://dx.doi.org/10.1039/c0ee00558d.

[12] G. Wu, P. Zelenay, Acc. Chem. Res. 46 (2013) 1878–1889, http://dx.doi.org/10.1021/ar400011z.

[13] K. Vignarooban, J. Lin, A. Arvay, S. Kolli, I. Kruusenberg, K. Tammeveski, L. Munukutla, A.M. Kannan, Chin. J. Catal. 36 (2015) 458–472, http://dx.doi.org/10.1016/S1872-2067(14)60175-3.

[14] T. Sun, Y. Jiang, Q. Wu, L. Du, Z. Zhang, L. Yang, X. Wang, Z. Hu, Catal. Sci. Technol. 7 (2017) 51–55, http://dx.doi.org/10.1039/C6CY01921H.

[15] T. Sun, Q. Wu, O. Zhuo, Y. Jiang, Y. Bu, L. Yang, X. Wang, Z. Hu, Nanoscale 8 (2016) 8480–8485, http://dx.doi.org/10.1039/C6NR00760 K.

[16] A.L. Dicks, J. Power Sources 156 (2006) 128–141, http://dx.doi.org/10.1016/j.jpowsour.2006.02.054.

[17] U.I. Kramm, M. Lefèvre, N. Larouche, D. Schmeisser, J.P. Dodelet, J. Am. Chem. Soc. 136 (2014) 978–985, http://dx.doi.org/10.1021/ja410076f.

[18] H.R. Byon, J. Suntivich, E.J. Crumlin, Y. Shao-Horn, Phys. Chem. Chem. Phys. 13 (2011) 21437–21445, http://dx.doi.org/10.1039/C1cp23029 h.

[19] B. Merzougui, A. Hachimi, A. Akinpelu, S. Bukola, M. Shao, Electrochim. Acta 107 (2013) 126–132, http://dx.doi.org/10.1016/j.electacta.2013.06.016.

[20] L. Osmieri, A.H.A. Monteverde Videla, S. Specchia, J. Power Sources 278 (2015) 296–307, http://dx.doi.org/10.1016/j.jpowsour.2014.12.080.

[21] B.J. Kim, D.U. Lee, J. Wu, D. Higgins, A. Yu, Z. Chen, J. Phys. Chem. C 117 (2013) 26501–26508, http://dx.doi.org/10.1021/jp410014a.

[22] C. Dominguez, F.J. Perez-Alonso, M.A. Salam, S.A. Al-Thabaiti, M.A. Pena, L. Barrio, S. Rojas, J. Mater. Chem. A 3 (2015) 24487–24494, http://dx.doi.org/10.1039/C5TA04355G.

[23] T. Kottakkat, M. Bron, ChemElectroChem 1 (2014) 2163–2171, http://dx.doi.org/10.1002/celc.201402231.

[24] J.K. Dombrovskis, A.E.C. Palmqvist, Fuel Cells 16 (2016) 23–31, http://dx.doi.org/10.1002/fuce.201500122.

[25] A. Sarapuu, L. Samolberg, K. Kreek, M. Koel, L. Matisen, K. Tammeveski, J. Electroanal. Chem. 746 (2015) 9–17, http://dx.doi.org/10.1016/j.jelechem.2015.03.021.

[26] K. Kreek, A. Sarapuu, L. Samolberg, U. Joost, V. Mikli, M. Koel, K. Tammeveski, ChemElectroChem 2 (2015) 2079–2088, http://dx.doi.org/10.1002/celc.201500275.

[27] A. Sarapuu, K. Kreek, K. Kisand, M. Kook, M. Uibu, M. Koel, K. Tammeveski, Electrochim. Acta 230 (2017) 81–88, http://dx.doi.org/10.1016/j.electacta.2017.01.157.

[28] A. Jänes, T. Thomberg, H. Kurig, E. Lust, Carbon 47 (2009) 23–29, http://dx.doi.org/10.1016/j.carbon.2008.07.010.

[29] R.K. Dash, G. Yushin, Y. Gogotsi, Microporous Mesoporous Mat. 86 (2005) 50–57, http://dx.doi.org/10.1016/j.micromeso.2005.05.047.

[30] M. Schmirler, T. Knorr, T. Fey, A. Lynen, P. Greil, B.J.M. Etzold, Carbon 49 (2011) 4359–4367, http://dx.doi.org/10.1016/j.carbon.2011.06.013.

[31] J. Leis, M. Arulepp, A. Perkson, Method to Modify Pore Characteristics of Porous Carbon and Porous Carbon Amterials Produced by the Same Method, 2004 (WO2004/094307).

[32] E. Lust, K. Vaarmets, J. Nerut, I. Tallo, P. Valk, S. Sepp, E. Härk, Electrochim. Acta 140 (2014) 294–303, http://dx.doi.org/10.1016/j.electacta.2014.04.054.

[33] R. Jäger, E. Härk, V. Steinberg, E. Lust, ECS Trans. 66 (2015) 47–55, http://dx.doi.org/10.1149/06624.0047ecst.

[34] R. Jäger, P.E. Kasatkin, E. Härk, E. Lust, Electrochem. Commun. 35 (2013) 97–99, http://dx.doi.org/10.1016/j.elecom.2013.08.001.

[35] I. Kruusenberg, J. Leis, M. Arulepp, K. Tammeveski, J. Solid State Electrochem. 14 (2010) 1269–1277, http://dx.doi.org/10.1007/s10008-009-0930-2.

[36] S. Kundu, W. Xia, W. Busser, M. Becker, D.A. Schmidt, M. Havenith, M. Muhler, Phys. Chem. Chem. Phys. 12 (2010) 4351–4359, http://dx.doi.org/10.1039/b923651a.

[37] T. Sharifi, G. Hu, X. Jia, T. Wågberg, ACS Nano 6 (2012) 8904–8912, http://dx.doi.org/10.1021/nn302906r.

[38] K. Gong, F. Du, Z. Xia, M. Durstock, L. Dai, Science 323 (2009) 760–764, http://dx.doi.org/10.1126/science.1168049.

[39] H. Li, W. Kang, L. Wang, Q. Yue, S. Xu, H. Wang, J. Liu, Carbon 54 (2013) 249–257, http://dx.doi.org/10.1016/j.carbon.2012.11.036.

[40] Y. Zhao, L. Yang, S. Chen, X. Wang, Y. Ma, Q. Wu, Y. Jiang, W. Qian, Z. Hu, J. Am. Chem. Soc. 135 (2013) 1201–1204, http://dx.doi.org/10.1021/ja310566z.

[41] K.H. Wu, D.W. Wang, D.S. Su, I.R. Gentle, ChemSusChem 8 (2015) 2772–2788, http://dx.doi.org/10.1002/cssc.201500373.

[42] D. Wei, Y. Liu, Y. Wang, H. Zhang, L. Huang, G. Yu, Nano Lett. 9 (2009) 1752–1758, http://dx.doi.org/10.1021/nl803279t.

[43] D. Long, W. Li, L. Ling, J. Miyawaki, I. Mochida, S.H. Yoon, Langmuir 26 (2010) 16096–16102, http://dx.doi.org/10.1021/la102425a.

[44] S. Ratso, I. Kruusenberg, U. Joost, R. Saar, K. Tammeveski, Int. J. Hydrogen Energy 41 (2016) 22510–22519, http://dx.doi.org/10.1016/j.ijhydene.2016.02.021.

[45] S. Ratso, I. Kruusenberg, M. Vikkisk, U. Joost, E. Shulga, I. Kink, T. Kallio, K. Tammeveski, Carbon 73 (2014) 361–370, http://dx.doi.org/10.1016/j.carbon.2014.02.076.

[46] N.P. Subramanian, X. Li, V. Nallathambi, S.P. Kumaraguru, H. Colon-Mercado, G. Wu, J.W. Lee, B.N. Popov, J. Power Sources 188 (2009) 38–44, http://dx.doi.org/10.1016/j.jpowsour.2008.11.087.

[47] X. Wang, Q. Li, H. Pan, Y. Lin, Y. Ke, H. Sheng, M.T. Swihart, G. Wu, Nanoscale 7 (2015) 20290–20298, http://dx.doi.org/10.1039/C5NR05864C.

[48] J. Zhang, Z. Zhao, Z. Xia, L. Dai, Nat. Nanotechnol. 10 (2015) 444–452, http://dx.doi.org/10.1038/nnano.2015.48.

[49] P.H. Matter, E. Wang, M. Arias, E.J. Biddinger, U.S. Ozkan, J. Mol. Catal. A Chem. 264 (2007) 73–81, http://dx.doi.org/10.1016/j.molcata.2006.09.008.

[50] G. Liu, X. Li, P. Ganesan, B.N. Popov, Electrochim. Acta 55 (2010) 2853–2858, http://dx.doi.org/10.1016/j.electacta.2009.12.055.

[51] M. Ferrandon, A.J. Kropf, D.J. Myers, K. Artyushkova, U. Kramm, P. Bogdanoff, G. Wu, C.M. Johnston, P. Zelenay, J. Phys. Chem. C 116 (2012) 16001–16013, http://dx.doi.org/10.1021/jp302396 g.

[52] U.I. Kramm, J. Herranz, N. Larouche, T.M. Arruda, M. Lefèvre, F. Jaouen, P. Bogdanoff, S. Fiechter, I. Abs-Wurmbach, S. Mukerjee, J.-P. Dodelet, Phys. Chem. Chem. Phys. 14 (2012) 11673–11688, http://dx.doi.org/10.1039/c2cp41957b.

[53] F. Jaouen, J. Herranz, M. Lefèvre, J.-P. Dodelet, U.I. Kramm, I. Herrmann, P. Bogdanoff, J. Maruyama, T. Nagaoka, A. Garsuch, J.R. Dahn, T. Olson, S. Pylypenko, P. Atanassov, E.A. Ustinov, ACS Appl. Mater. Interfaces 1 (2009) 1623–1639, http://dx.doi.org/10.1021/am900219 g.

[54] K. Strickland, E. Miner, Q. Jia, U. Tylus, N. Ramaswamy, W. Liang, M. Sougrati, F. Jaouen, S. Mukerjee, Nat. Commun. 6 (2015) 7343, http://dx.doi.org/10.1038/ncomms8343.

[55] M. Shao, Q. Chang, J.-P. Dodelet, R. Chenitz, Chem. Rev. 116 (2016) 3594–3657, http://dx.doi.org/10.1021/acs.chemrev.5b00462.

[56] S. Ratso, I. Kruusenberg, M. Käärik, M. Kook, R. Saar, M. Pärs, J. Leis, K. Tammeveski, Carbon 113 (2017) 159–169, http://dx.doi.org/10.1016/j.carbon.2016.11.037.

[57] S. Ratso, I. Kruusenberg, A. Sarapuu, P. Rauwel, R. Saar, U. Joost, J. Aruväli, P. Kanninen, T. Kallio, K. Tammeveski, J. Power Sources 332 (2016) 129–138, http://dx.doi.org/10.1016/j.jpowsour.2016.09.069.

[58] S. Ratso, I. Kruusenberg, A. Sarapuu, M. Kook, P. Rauwel, R. Saar, J. Aruväli, K. Tammeveski, Electrochim. Acta 218 (2016) 303–310, http://dx.doi.org/10.1016/j.electacta.2016.09.119.

[59] I. Kruusenberg, D. Ramani, S. Ratso, U. Joost, R. Saar, P. Rauwel, A.M. Kannan, K. Tammeveski, ChemElectroChem 3 (2016) 1455–1465, http://dx.doi.org/10.1002/celc.201600241.

[60] M. Thommes, K. Kaneko, A.V. Neimark, J.P. Olivier, F. Rodriguez-Reinoso, J. Rouquerol, K.S.W. Sing, Pure Appl. Chem. 87 (2015) 1051–1069, http://dx.doi.org/10.1515/pac-2014-1117.

[61] F. Jaouen, J. Herranz, M. Lefèvre, J.P. Dodelet, U.I. Kramm, I. Herrmann, P. Bogdanoff, J. Maruyama, T. Nagaoka, A. Garsuch, J.R. Dahn, T. Olson, S. Pylypenko, P. Atanassov, E.A. Ustinov, ACS Appl. Mater. Interfaces 1 (2009) 1623–1639, http://dx.doi.org/10.1021/am900219 g.

[62] H.W. Liang, W. Wei, Z.S. Wu, X. Feng, K. Müllen, J. Am. Chem. Soc. 135 (2013) 16002–16005, http://dx.doi.org/10.1021/ja407552k.

[63] A.J. Bard, L.R. Faulkner, Electrochemical Methods, 2nd ed., Wiley, New York, 2001.

[64] R.E. Davis, G.L. Horvath, C.W. Tobias, Electrochim. Acta 12 (1967) 287–297, http://dx.doi.org/10.1016/0013-4686(67)80007-0.

[65] D.R. Lide, CRC Handbook of Chemistry and Physics, 90th ed., CRC Press, Boca Raton, 2009, http://dx.doi.org/10.1021/ja906434c.

[66] A. Brouzgou, S. Song, Z.-X. Liang, P. Tsiakaras, Catalysts 6 (2016) 159, http://dx.doi.org/10.3390/catal6100159.
[67] Y. Nie, L. Li, Z. Wei, Chem. Soc. Rev. 44 (2015) 2168–2201, http://dx.doi.org/10.1039/C4CS00484A.
[68] R. Jiang, D. Chu, J. Power Sources 245 (2014) 352–361, http://dx.doi.org/10.1016/j.jpowsour.2013.06.123.
[69] R. Gokhale, Y. Chen, A. Serov, K. Artyushkova, P. Atanassov, Electrochem. Commun. 72 (2016) 140–143, http://dx.doi.org/10.1016/j.elecom.2016.09.013.
[70] L. Ge, Y. Yang, L. Wang, W. Zhou, R. De Marco, Z. Chen, J. Zou, Z. Zhu, Carbon 82 (2015) 417–424, http://dx.doi.org/10.1016/j.carbon.2014.10.085.
[71] T. Sun, L. Xu, S. Li, W. Chai, Y. Huang, Y. Yan, J. Chen, Appl. Catal. B Environ. 193 (2016) 1–8, http://dx.doi.org/10.1016/j.apcatb.2016.04.006.
[72] Y. Sun, J. Wu, J. Tian, C. Jin, R. Yang, Electrochim. Acta 178 (2015) 806–812, http://dx.doi.org/10.1016/j.electacta.2015.08.059.
[73] S. Fu, C. Zhu, H. Li, D. Du, Y. Lin, J. Mater. Chem. A 3 (2015) 12718–12722, http://dx.doi.org/10.1039/C5TA01293G.
[74] M. Ahmed, I. Dincer, Int. J. Energy Res. 35 (2011) 1213–1228, http://dx.doi.org/10.1002/er.1889.
[75] G.K.S. Prakash, F.C. Krause, F.A. Viva, S.R. Narayanan, G.A. Olah, J. Power Sources 196 (2011) 7967–7972, http://dx.doi.org/10.1016/j.jpowsour.2011.05.056.
[76] X. Yan, Z. Tang, X. Xu, F. Fang, D. Song, J. Liu, S. Lu, L.-M. Liu, J. Luo, J. Zhu, Nano Energy 21 (2016) 265–275, http://dx.doi.org/10.1016/j.nanoen.2016.01.030.
[77] X. Sun, Y. Zhang, P. Song, J. Pan, L. Zhuang, W. Xu, W. Xing, ACS Catal. 3 (2013) 1726–1729, http://dx.doi.org/10.1021/cs400374k.
[78] X. Sun, P. Song, Y. Zhang, C. Liu, W. Xu, W. Xing, Sci. Rep. 3 (2013) 9603–9607, http://dx.doi.org/10.1038/srep02505.
[79] S. Zhao, H. Yin, L. Du, L. He, K. Zhao, L. Chang, G. Yin, H. Zhao, S. Liu, Z. Tang, ACS Nano 8 (2014) 12660–12668, http://dx.doi.org/10.1021/nn505582e.
[80] G.K. Goswami, R. Nandan, B.K. Barman, K.K. Nanda, J. Mater, Chem. A 1 (2013) 3133, http://dx.doi.org/10.1039/c2ta01129 h.
[81] S.J. Lue, W.-H. Pan, C.-M. Chang, Y.-L. Liu, J. Power Sources 202 (2012) 1–10, http://dx.doi.org/10.1016/j.jpowsour.2011.10.091.
[82] I. Kruusenberg, S. Ratso, M. Vikkisk, P. Kanninen, T. Kallio, A.M. Kannan, K. Tammeveski, J. Power Sources 281 (2015) 94–102, http://dx.doi.org/10.1016/j.jpowsour.2015.01.167.
[83] M. Borghei, P. Kanninen, M. Lundahl, T. Susi, J. Sainio, I. Anoshkin, A. Nasibulin, T. Kallio, K. Tammeveski, E. Kauppinen, V. Ruiz, Appl. Catal. B Environ. 158-159 (2014) 233–241, http://dx.doi.org/10.1016/j.apcatb.2014.04.027.
[84] P. Kanninen, M. Borghei, O. Sorsa, E. Pohjalainen, E.I. Kauppinen, V. Ruiz, T. Kallio, Appl. Catal. B Environ. 156-157 (2014) 341–349, http://dx.doi.org/10.1016/j.apcatb.2014.03.041.
[85] M. Lei, J. Wang, J.R. Li, Y.G. Wang, H.L. Tang, W.J. Wang, Sci. Rep. 4 (2014) 6013, http://dx.doi.org/10.1038/srep06013.
[86] R. Janarthanan, A. Serov, S.K. Pilli, D.A. Gamarra, P. Atanassov, M.R. Hibbs, A.M. Herring, Electrochim. Acta 175 (2015) 202–208, http://dx.doi.org/10.1016/j.electacta.2015.03.209.
[87] D. Sebastián, A. Serov, I. Matanovic, K. Artyushkova, P. Atanassov, A.S. Aricò, V. Baglio, Nano Energy 34 (2017) 195–204, http://dx.doi.org/10.1016/j.nanoen.2017.02.039.
[88] D. Sebastián, V. Baglio, A.S. Aricò, A. Serov, P. Atanassov, Appl. Catal. B Environ. 182 (2016) 297–305, http://dx.doi.org/10.1016/j.apcatb.2015.09.043.
[89] D. Sebastián, A. Serov, K. Artyushkova, P. Atanassov, A.S. Aricò, V. Baglio, J. Power Sources 319 (2016) 235–246, http://dx.doi.org/10.1016/j.jpowsour.2016.04.067.
[90] D. Sebastián, A. Serov, K. Artyushkova, J. Gordon, P. Atanassov, A.S. Aricò, V. Baglio, ChemSusChem 9 (2016) 1986–1995, http://dx.doi.org/10.1002/cssc.201600583.